NACA RM E54G07

NACA

RESEARCH MEMORANDUM

INVESTIGATION OF NOISE FIELD AND VELOCITY PROFILES OF AN AFTERBURNING ENGINE

By Warren J. North, Edmund E. Callaghan, and Chester D. Lanzo

Lewis Flight Propulsion Laboratory
Cleveland, Ohio

NATIONAL ADVISORY COMMITTEE FOR AERONAUTICS

WASHINGTON

September 24, 1954

NATIONAL ADVISORY COMMITTEE FOR AERONAUTICS

RESEARCH MEMORANDUM

INVESTIGATION OF NOISE FIELD AND VELOCITY PROFILES OF AN AFTERBURNING ENGINE

By Warren J. North, Edmund E. Callaghan, and Chester D. Lanzo

SUMMARY

Sound pressure levels, frequency spectrum, and jet velocity profiles are presented for an engine-afterburner combination at various values of afterburner fuel-air ratio. At the high fuel-air ratios, severe low-frequency resonance was encountered which represented more than half the total energy in the sound spectrum. At similar thrust conditions, lower sound pressure levels were obtained from a current fighter aircraft with a different afterburner configuration. The lower sound pressure levels are attributed to resonance-free afterburner operation and thereby indicate the importance of acoustic considerations in afterburner design.

CH-1

INTRODUCTION

The operation of high-performance afterburner-equipped jet aircraft from airports located in or near densely populated residential areas represents a formidable noise problem. Much higher noise levels generated by afterburner-equipped aircraft have not only increased public indignation toward jet noise but have also created a serious noise problem to supporting personnel at engine test facilities and aboard aircraft carriers. Afterburning thrust augmentation produces higher noise levels primarily because of the high jet velocities associated with increased jet temperatures and secondly because of the increased diameter of the jet nozzle.

Recent investigations (refs. 1 to 3) show that, for the range of jet pressure ratios of current interest, noise generation results largely from the turbulent mixing of the exhaust jet with the surrounding atmosphere. Lighthill (ref. 4) has shown theoretically that the over-all radiated sound power from a jet discharging into quiescent air varies directly as the eighth power of the jet velocity and the square of the jet diameter. Model jet investigations (ref. 2) report excellent agreement with the Lighthill theory. Experimental investigations of over-all

sound power radiated from turbojet engines (refs. 1 and 2) show good agreement, in general, with the Lighthill theory. Reference 2 shows some disagreement with the eighth-power relation for full-scale engines at low engine power and consequent low jet velocities. This discrepancy at low velocities is partially attributed to the fact that compressor noise has become an appreciable portion of over-all noise.

The investigation of the noise field in the vicinity of an afterburner-equipped engine reported herein was conducted at the NACA Lewis laboratory and represents a portion of a study of jet noise and means for its suppression.

APPARATUS AND PROCEDURE

The engine and afterburner configuration used in this investigation was mounted beneath the wing of a C-82 aircraft, as shown in figure 1. The area where the tests were conducted is unobstructed rearward and to the sides of the aircraft for over 1/2 mile. The nearest reflecting surface other than the aircraft surfaces was located approximately 600 feet in front of the aircraft. Measurements of the over-all sound pressure level were made approximately 6 feet above ground level at 15° intervals from the jet axis and 200 feet from the jet nozzle, as shown in figure 2. Sound-pressure-level measurements were made with a General Radio Company Type 1551-A Sound Level Meter. The frequency distribution of the noise was measured at stations 45° and 90° from the jet axis (fig. 2) at a distance of 200 feet from the jet exit. The frequency distribution was measured with a Brüel and Kjaer Audio Frequency Spectrum Recorder Type 2311. The frequency range for this instrument is from 35 to 18,000 cycles per second and is divided into 27 one-third octaves.

The sound field was surveyed by obtaining measurements of sound pressure level at each of the stations shown in figure 2 at rated engine speed and for afterburner fuel-air ratios from zero to 0.0274, which correspond approximately to engine over-all fuel-air ratios of 0.015 to 0.042. The frequency spectrum was measured at one station simultaneously with the over-all field survey. Each set of measurements required approximately 3 minutes.

The jet engine used in this investigation was an axial-flow engine with a rated sea-level static thrust of 5000 pounds and a turbine-outlet temperature of 690° C. The afterburner used in the investigation is shown in figure 3. The afterburner was essentially 32 inches in diameter and 54 inches long with a fixed-area nozzle $25\frac{1}{4}$ inches in diameter. The flame holder was a conventional double-ring V-gutter type.

The total-pressure and temperature distributions across the vertical center line of the nozzle from the jet axis to the nozzle lip were measured with two specially built water-cooled pressure and temperature probes (fig. 4). Details of the probe tips are shown in figure 4(b). The tip or head of the pressure probe is essentially a blunt-nosed wedge with a total-pressure hole in the leading edge and an orifice on each face of the wedge for measuring flow angularity. The tip of the temperature probe is a U-shaped platinum - platinum-rhodium thermocouple. The conduction error of this couple was determined from the base temperatures measured by a platinum wire connected to the platinum-rhodium side of the main couple and a platinum-rhodium wire connected to the platinum side (fig. 4(b)). The probes were moved across the jet exit from the jet center line to the nozzle lip by means of an actuator mounted on top of the afterburner (fig. 5).

For comparison, the sound field and frequency spectrum of a current afterburner-equipped fighter aircraft were measured. These data were obtained with the exit nozzle of the fighter in the same location of the sound field as the exit nozzle of the test engine previously described.

CH-1 back

RESULTS AND DISCUSSION

The afterburner utilized in this investigation was constructed with a fixed-area nozzle. The pumping characteristics of a turbojet engine are such that, at rated engine speed, only one afterburner fuel-air ratio yields rated turbine-discharge temperature and hence maximum over-all engine pressure ratio. At lower afterburner fuel-air ratios, both the turbine-discharge temperature and the over-all engine pressure ratio will be decreased. Although this type of afterburner operation is unconventional, it does not affect the principal parameters of afterburner sound generation.

Jet Temperature

Figure 6 shows the relation between indicated probe temperatures and corrected jet total temperatures across the nozzle radius at an afterburner fuel-air ratio of 0.0234. The jet total temperature was obtained by correcting for radiation, conduction, and thermocouple recovery by methods outlined in references 5 and 6. The maximum total temperature was 400° higher than the measured temperature at the main-junction thermocouple. At this probe location, the base-junction temperature was 600° lower than that at the main junction.

The corrected total-temperature profiles for the entire range of afterburner fuel-air ratios from zero to 0.0274 are shown in figure 7. At the higher fuel-air ratios, the temperature in the core of the jet is

seen to be much higher than in the outer regions of the jet. At the lower temperatures, the profile is uniform except at the jet boundary. The low temperatures corresponding to low fuel-air ratios are below turbine-outlet rated temperature, as would be expected, because the engine is operating with constant exhaust-nozzle area. Rated turbine-outlet temperature was attained only at an afterburner fuel-air ratio of 0.0274. No temperature measurements were taken in the core of the jet at the maximum fuel-air ratio because the temperature of the main junction was approaching the melting point of platinum.

Jet Mach Number and Velocity

The radial distribution of Mach number is shown in figure 8 for a range of afterburner fuel-air ratios from zero to 0.0274. The Mach number was a maximum near the nozzle lip and increased with increasing fuel-air ratios. More uniform Mach number profiles occur at the higher fuel-air ratios. As would be expected, the large variation of Mach number with fuel-air ratio was due to the constant-area exhaust nozzle, because engine pressure ratio decreased considerably as afterburner fuel-air ratio decreased. Constant free-stream static pressure across the subsonic jet was assumed for the Mach number calculations. Small total-pressure corrections due to jet swirl were necessary at the low pressure ratios.

The velocity profiles, which were computed from the temperature and Mach number data, are shown in figure 9. At the high fuel-air ratios, the velocity is maximum and the profile is nearly flat over the center half of the jet and decreases near the lip. At the low fuel-air ratios, the velocity profiles are similar to the Mach number profiles because temperature distribution is uniform across the main portion of the jet.

The mass-flow-weighted average velocity for each afterburner fuel-air ratio was computed from the curves of figure 9, and the values are shown in the following table:

Afterburner fuel-air ratio, lb fuel/lb air	Mass-flow-weighted average velocity, ft/sec
0	945
.0075	970
.0125	1068
.0177	1500
.0234	1802
.0274	2100

Sound Measurements

The frequency distribution of the jet noise at 45° and 90° azimuth angles and at a distance of 200 feet from the jet exit is shown in figure 10, where the spectrum level (sound power per cycle) is plotted as a function of frequency. It is apparent that most of the sound energy at 45° azimuth angle occurs at frequencies below 500 cycles per second (fig. 10(a)), and at 90° azimuth angle, most of the energy exists below 1000 cycles per second (fig. 10(b)). In addition, at both azimuth angles, a strong resonant condition exists at approximately 80 cycles per second for the high fuel-air ratios. The low frequency of the resonance infers a longitudinal mode of vibration, since the corresponding wave length is approximately twice the length of the engine and afterburner. At the three highest fuel-air ratios, the energy in the third octave band centered around 80 cycles per second is approximately 50 percent or more of the total energy in the entire spectrum. Since the peak decibel values at the resonant condition are nearly the same for the three highest fuel-air ratios, it would be expected that the over-all sound pressure level throughout the entire field is greatly influenced by the resonance. The polar diagram of the sound field (fig. 11) bears out this conclusion, since the three highest fuel-air ratios show only a slight tendency of decreasing sound pressure level with decreasing fuel flow, that is, decreasing jet velocity. The sudden reduction in total sound power between a fuel-air ratio of 0.0177 and 0.0125 corresponds to the large reduction in the resonant condition shown by the spectrum-level curves (fig. 10).

It is therefore apparent that the effect of the resonance is so large as to preclude a correlation of the over-all integrated sound power level with the eighth-power law of Lighthill (ref. 4) mentioned previously. However, the spectrum levels at the 45° azimuth angle were integrated with a straight line between 63 and 100 cycles per second, with resonant condition ignored. The over-all sound pressure level obtained in this manner is shown as a function of the jet velocity in figure 12. Also in figure 12 are several points for the same engine with a standard tail pipe. These data are corrected to a diameter equal to the diameter of the afterburner nozzle.

The agreement between the two sets of data is quite good (within 2 db), and the slopes of both curves follow approximately a 6.25-power law of sound power with velocity. This deviation from the eighth-power law of Lighthill is not believed to be significant, since only one point in the field is being considered and not the total integrated power.

The undesirability of the resonance previously described cannot be overemphasized, not only with respect to noise but also from structural considerations. Operation of the present afterburner in the resonant condition resulted in a number of fatigue failures of the flame holder.

Fortunately, there are a number of remedies for all the various modes of afterburner resonance, and production afterburners are usually resonance-free. An example of a typical frequency spectrum of a current afterburner-equipped fighter airplane is shown in figure 13. These data were obtained at the same location and under similar atmospheric conditions as the results previously given. The aircraft incorporated the same type engine as that used in the previous tests but was fitted with a longer afterburner, which contained an inner liner and an electronically-controlled variable-area nozzle. The spectrum levels shown were measured at the 45° and 90° azimuth angles at 200 feet. A polar plot of the sound field is shown in figure 14. These measurements were made at the maximum thrust condition. The lack of any prominent resonances is quite apparent in figure 13. As a result, the over-all sound pressure field produces lower sound pressure levels than those obtained in the previous investigation.

SUMMARY OF RESULTS

As part of a program for the investigation of jet noise and means for its suppression, the sound field about an afterburner-equipped engine was investigated. Afterburner jet velocity profiles are presented from measurements made with water-cooled temperature and pressure probes. The particular configuration tested was found to have a strong resonance of approximately 80 cycles per second for a range of afterburner fuel-air ratios from zero to 0.0274. The sound power of the resonance was 50 percent or more of the total energy in the sound spectrum. Such a condition is highly undesirable with respect to engine noise and structural integrity of the engine and airframe. Integration of the sound spectrum at the 45° azimuth angle ignoring the resonant condition gave values of over-all sound pressure level which, when plotted against jet velocity, gave good agreement between afterburning and nonafterburning conditions.

The afterburner used in these tests was not representative of current production. Consequently, the sound field of a current afterburner-equipped aircraft was measured. The frequency spectrum was resonance-free and the sound levels were lower than for the experimental afterburner.

Lewis Flight Propulsion Laboratory
National Advisory Committee for Aeronautics
Cleveland, Ohio, July 8, 1954

REFERENCES

1. Callaghan, Edmund E., Howes, Walton, and North, Warren: Tooth-Type Noise-Suppression Devices on a Full-Scale Axial-Flow Turbojet Engine. NACA RM E54B01, 1954.

2. Tyler, John M., and Perry, Edward C.: Jet Noise. Preprint No. 287, SAE, Apr. 1954.

3. Lassiter, Leslie W., and Hubbard, Harvey H.: Experimental Studies of Noise from Subsonic Jets in Still Air. NACA TN 2757, 1952.

4. Lighthill, M. J.: On Sound Generated Aerodynamically. I - General Theory. Proc. Roy. Soc. (London), ser. A, vol. 211, no. 1107, Mar. 20, 1952, pp. 564-587.

5. Scadron, Marvin D., and Warshawsky, Isidore: Experimental Determination of Time Constants and Nusselt Numbers for Bare-Wire Thermocouples in High-Velocity Air Streams and Analytic Approximation of Conduction and Radiation Errors. NACA TN 2599, 1952.

6. Glawe, George E., and Shepard, Charles E.: Some Effects of Exposure to Exhaust-Gas Streams on Emittance and Thermoelectric Power of Bare-Wire Platinum Rhodium - Platinum Thermocouples. NACA TN 3253, 1954.

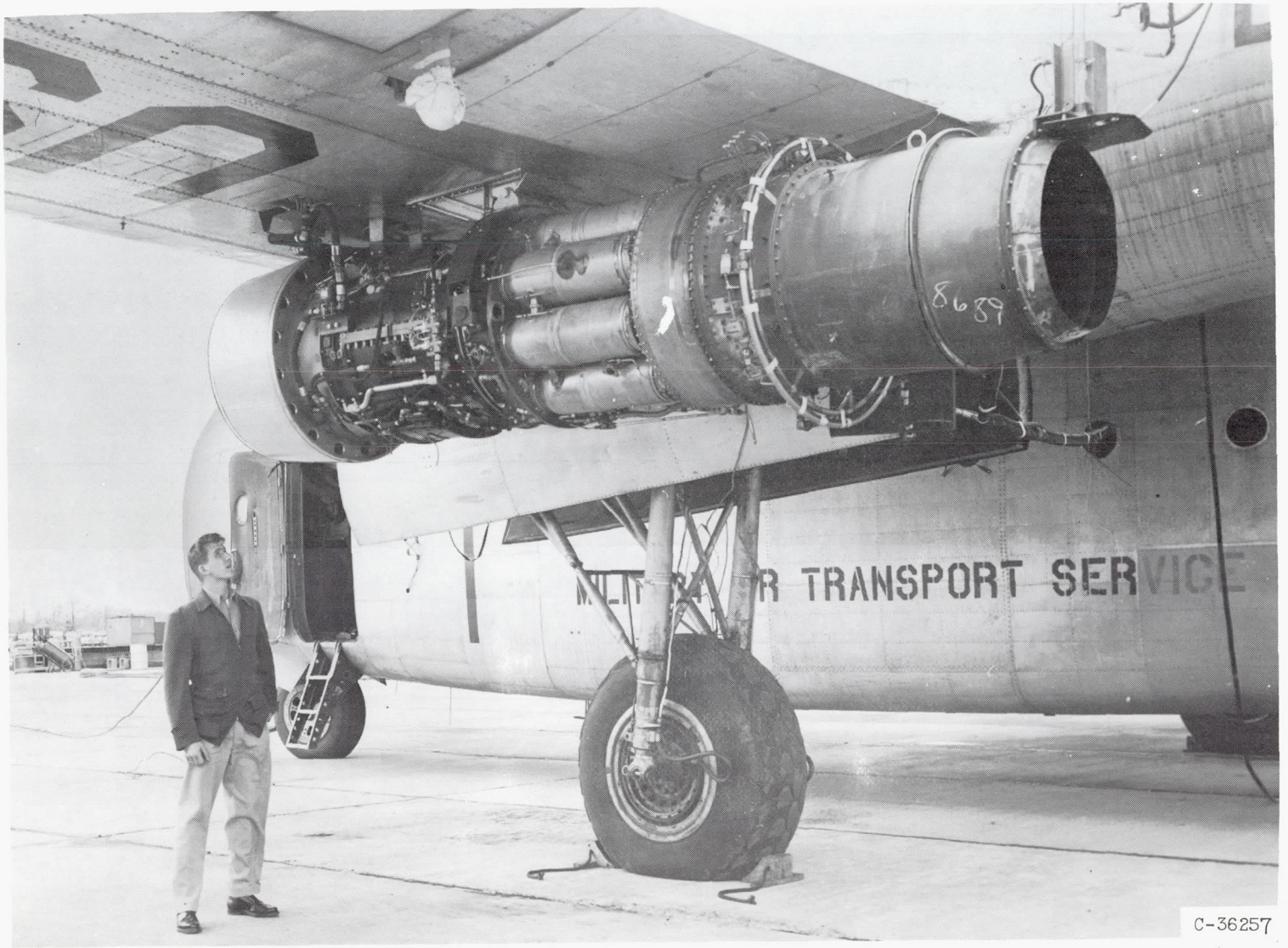

Figure 1. - Location of engine and afterburner beneath wing of cargo airplane.

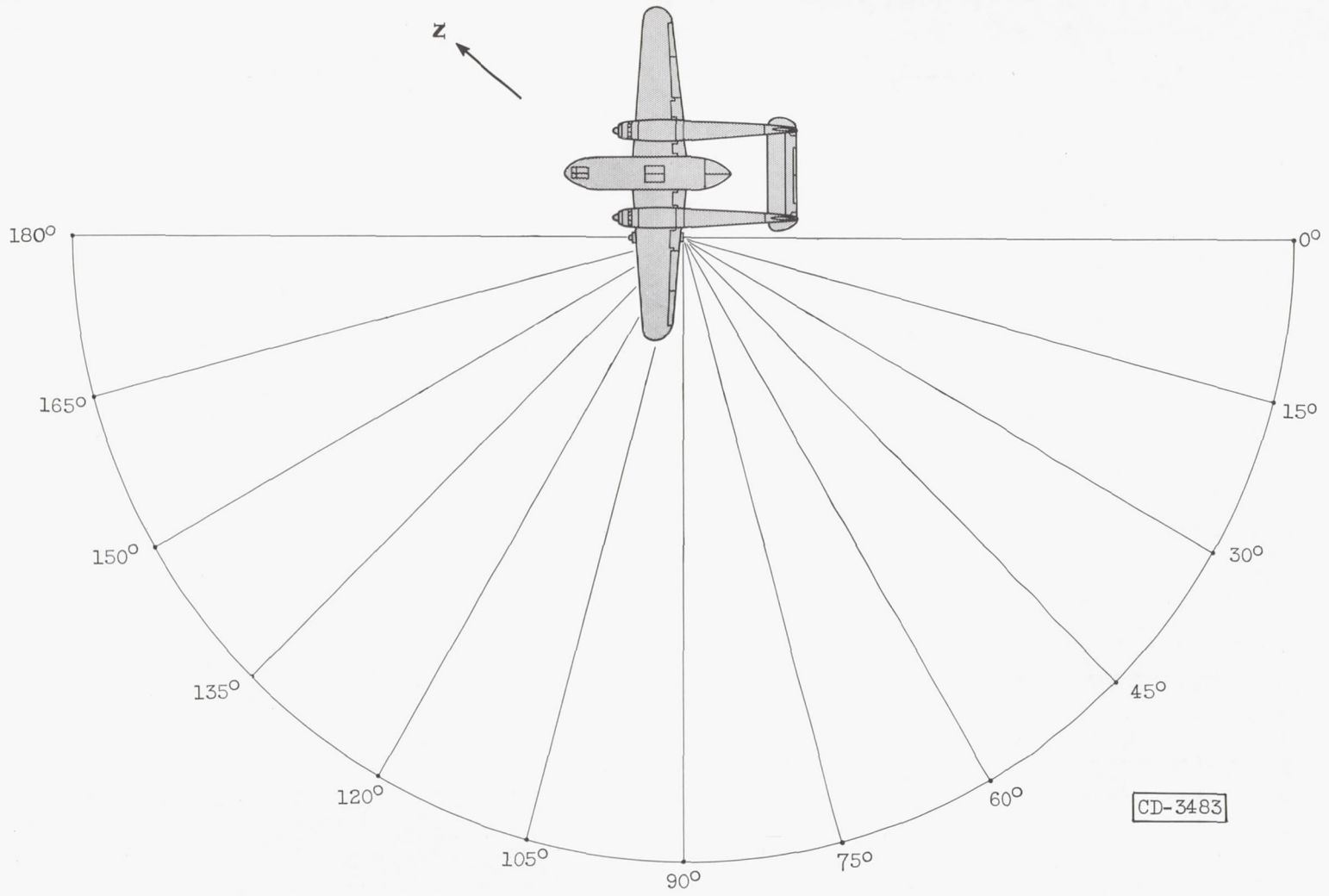

Figure 2. - Location of survey stations in sound field around aircraft test bed. Radius, 200 feet.

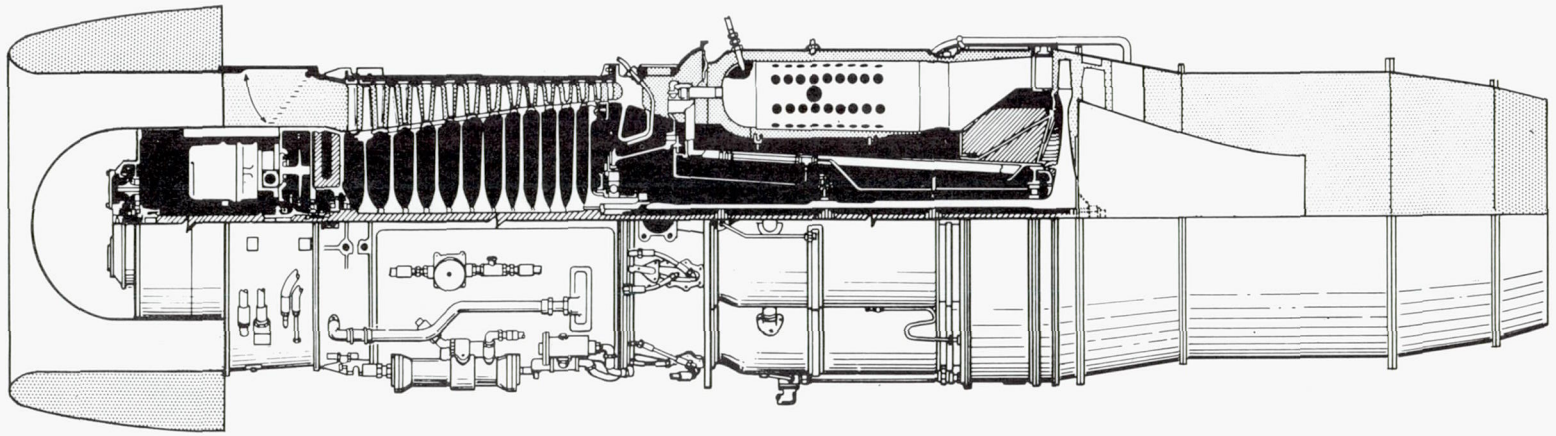

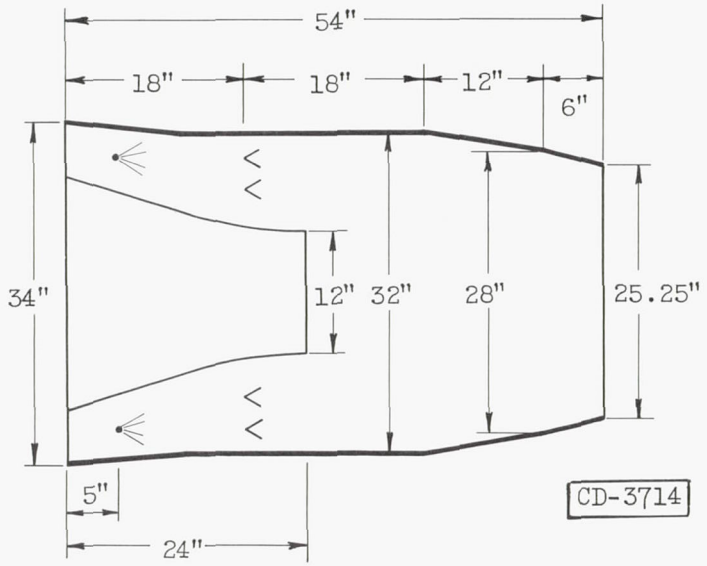

Figure 3. - Engine and afterburner installation.

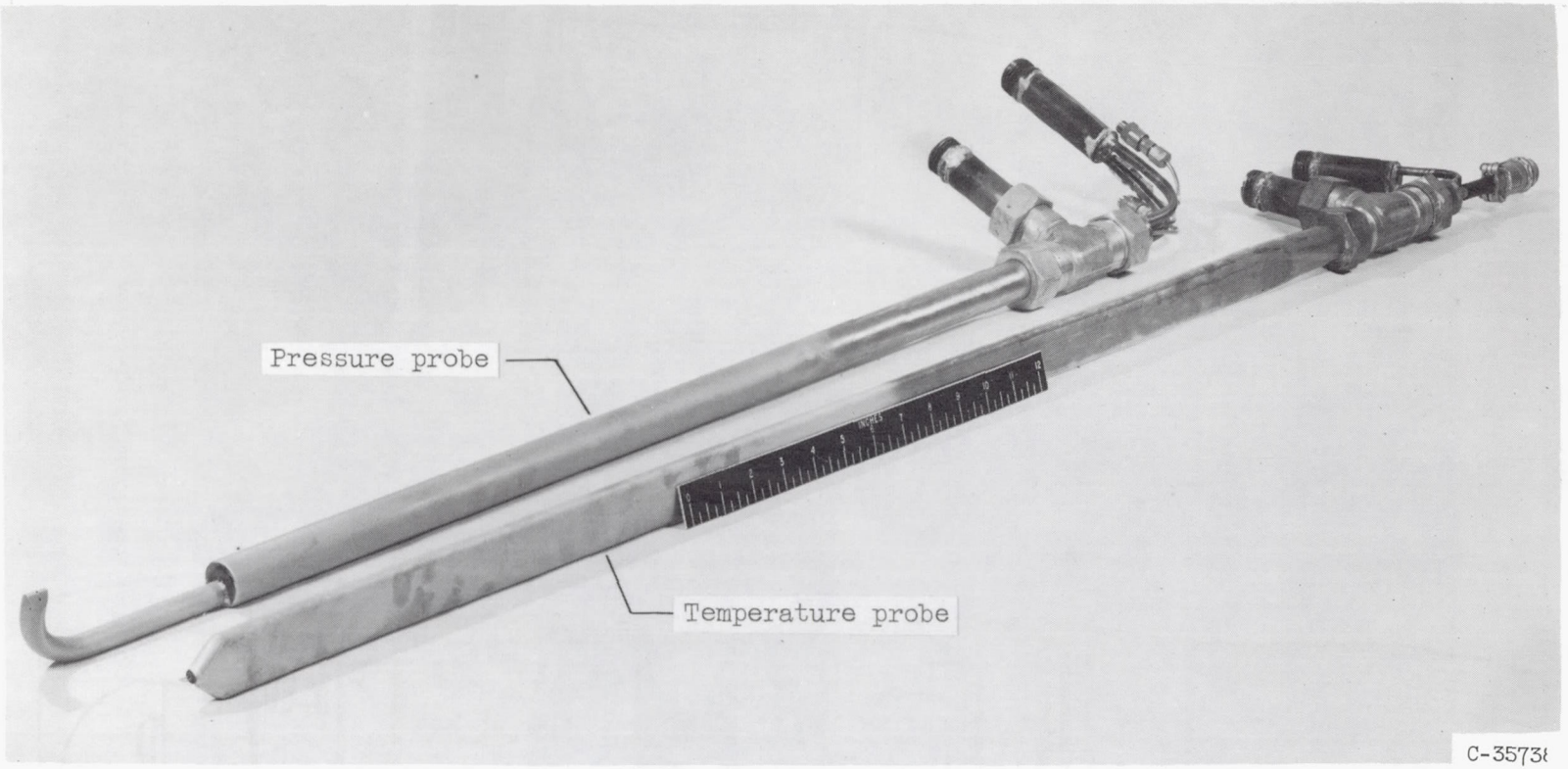

(a) Probes and water-cooling connectors.

Figure 4. - Water-cooled total-pressure and -temperature probes.

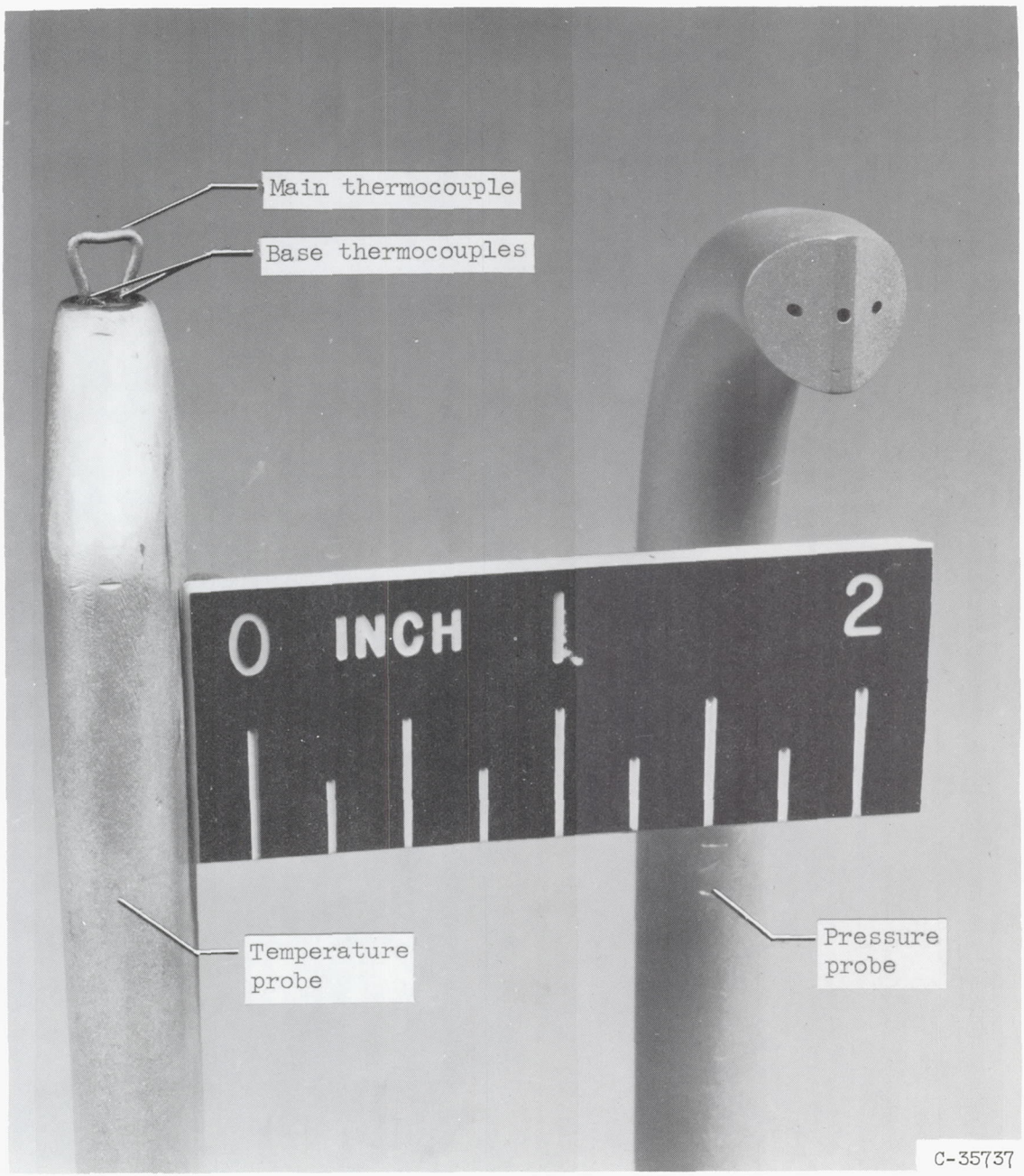

(b) Close-up of probe tips.

Figure 4. - Concluded. Water-cooled total-pressure and -temperature probes.

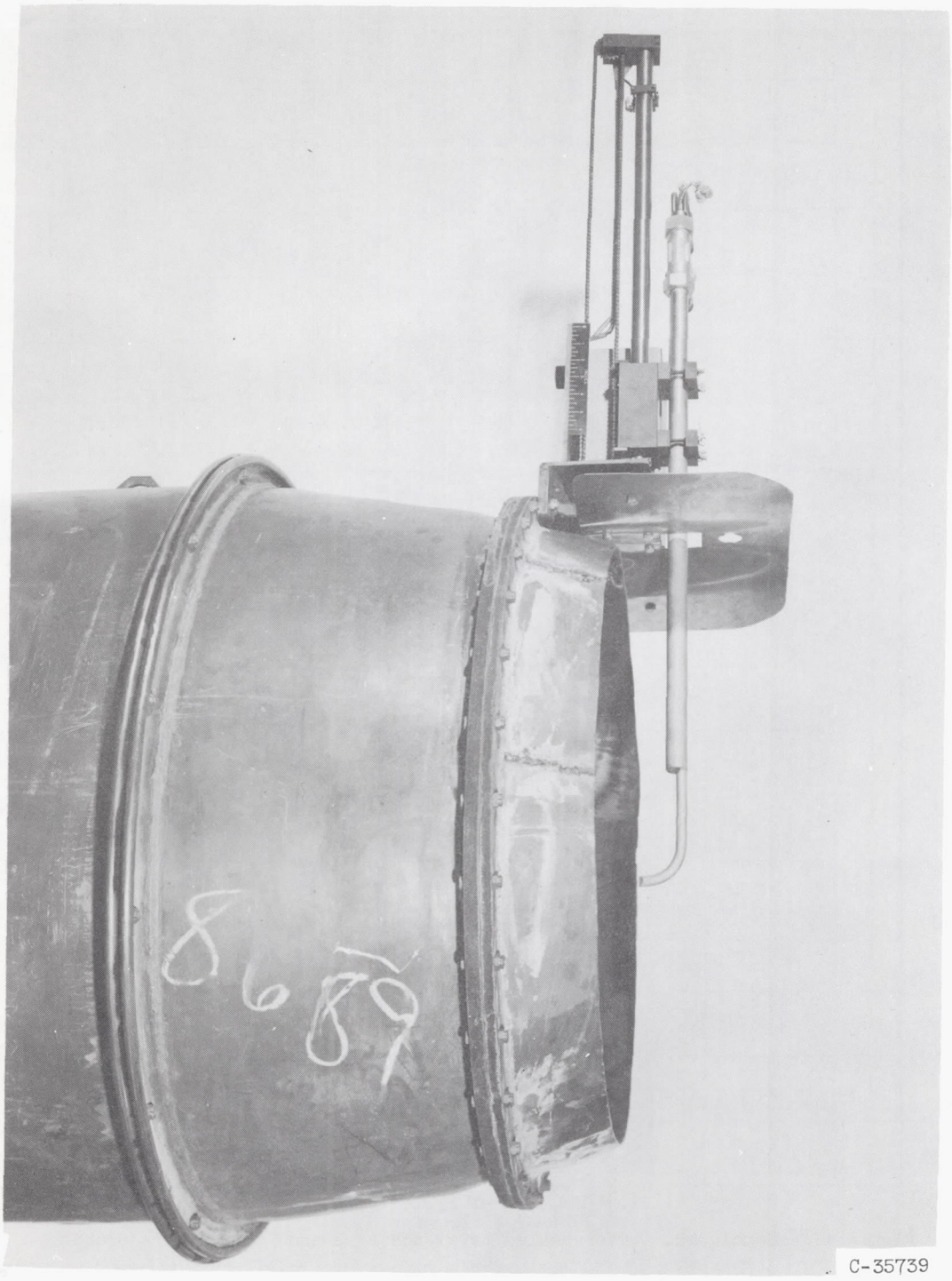

Figure 5. - Probe actuator mounted on afterburner.

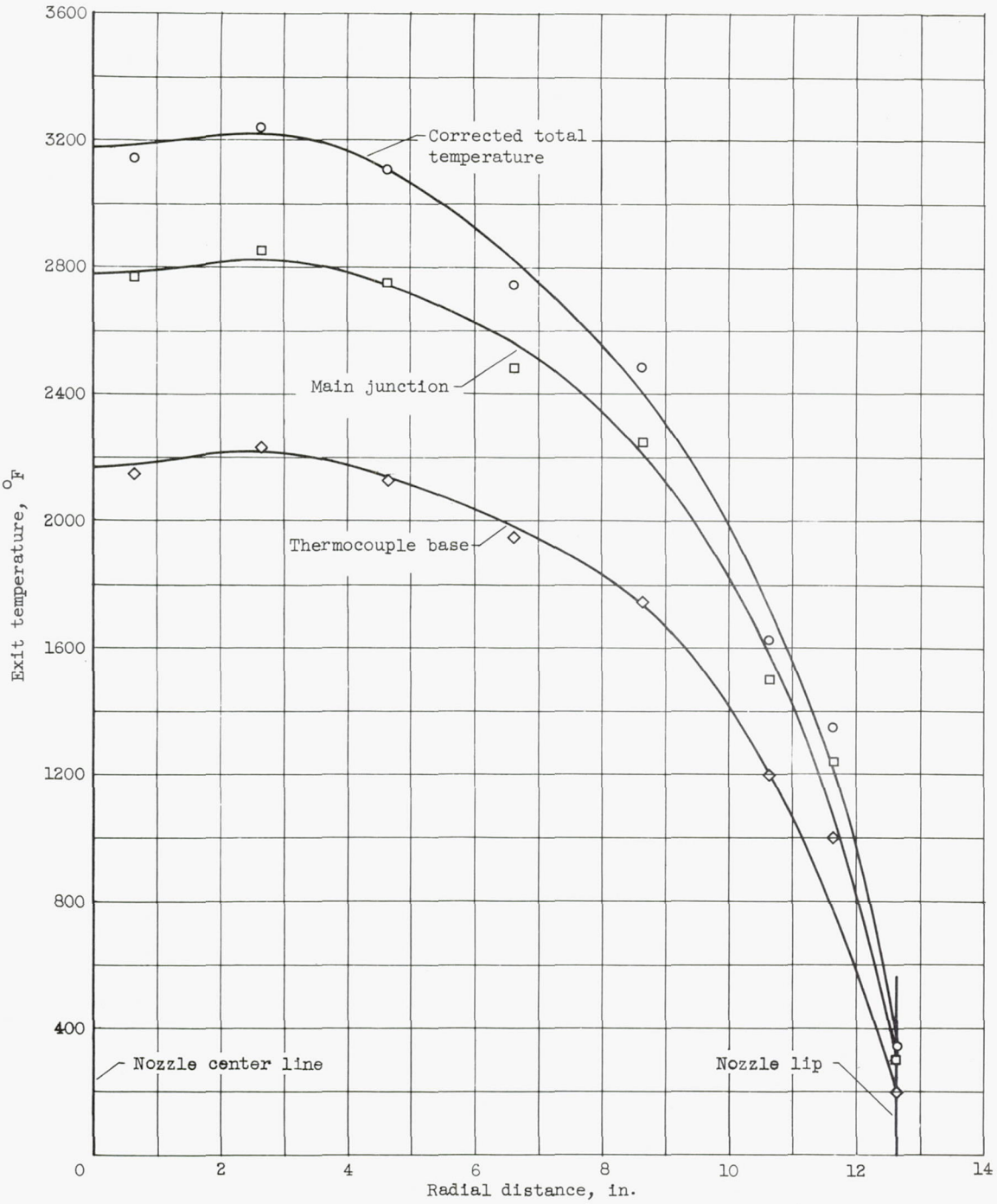

Figure 6. - Temperature profiles at afterburner-nozzle exit. Fuel-air ratio, 0.0234.

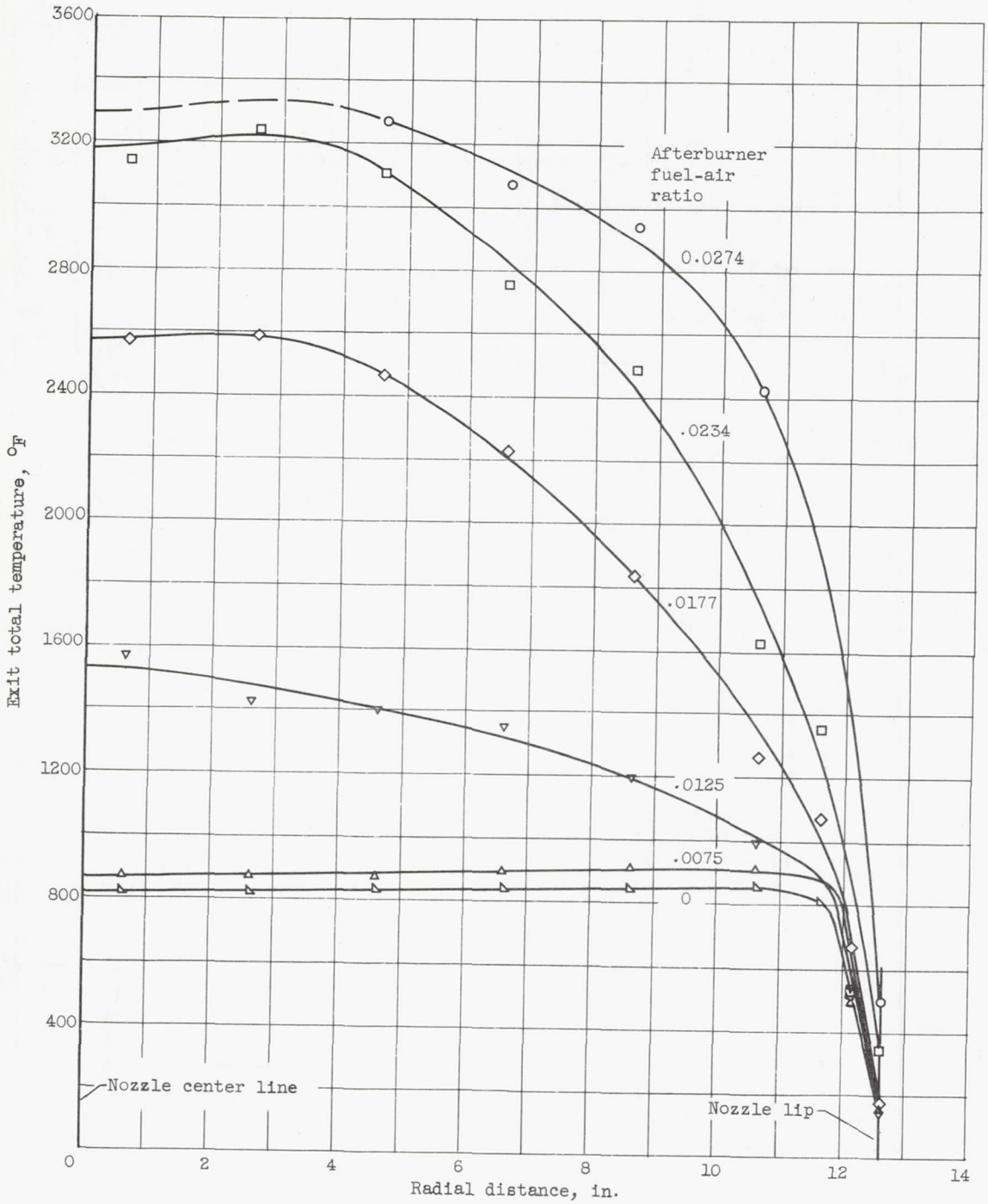

Figure 7. - Total-temperature profiles at afterburner-nozzle exit.

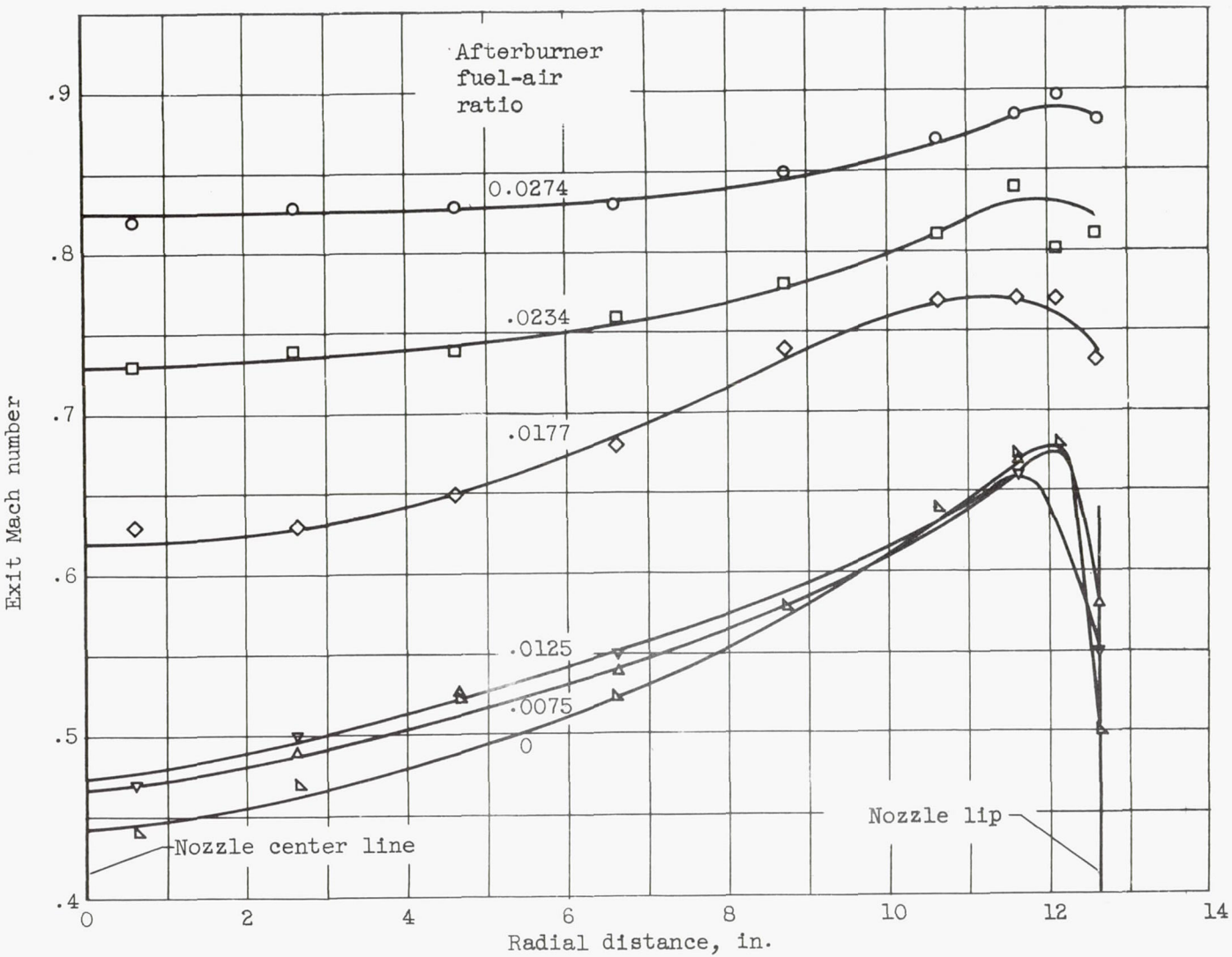

Figure 8. - Mach number profiles at afterburner-nozzle exit.

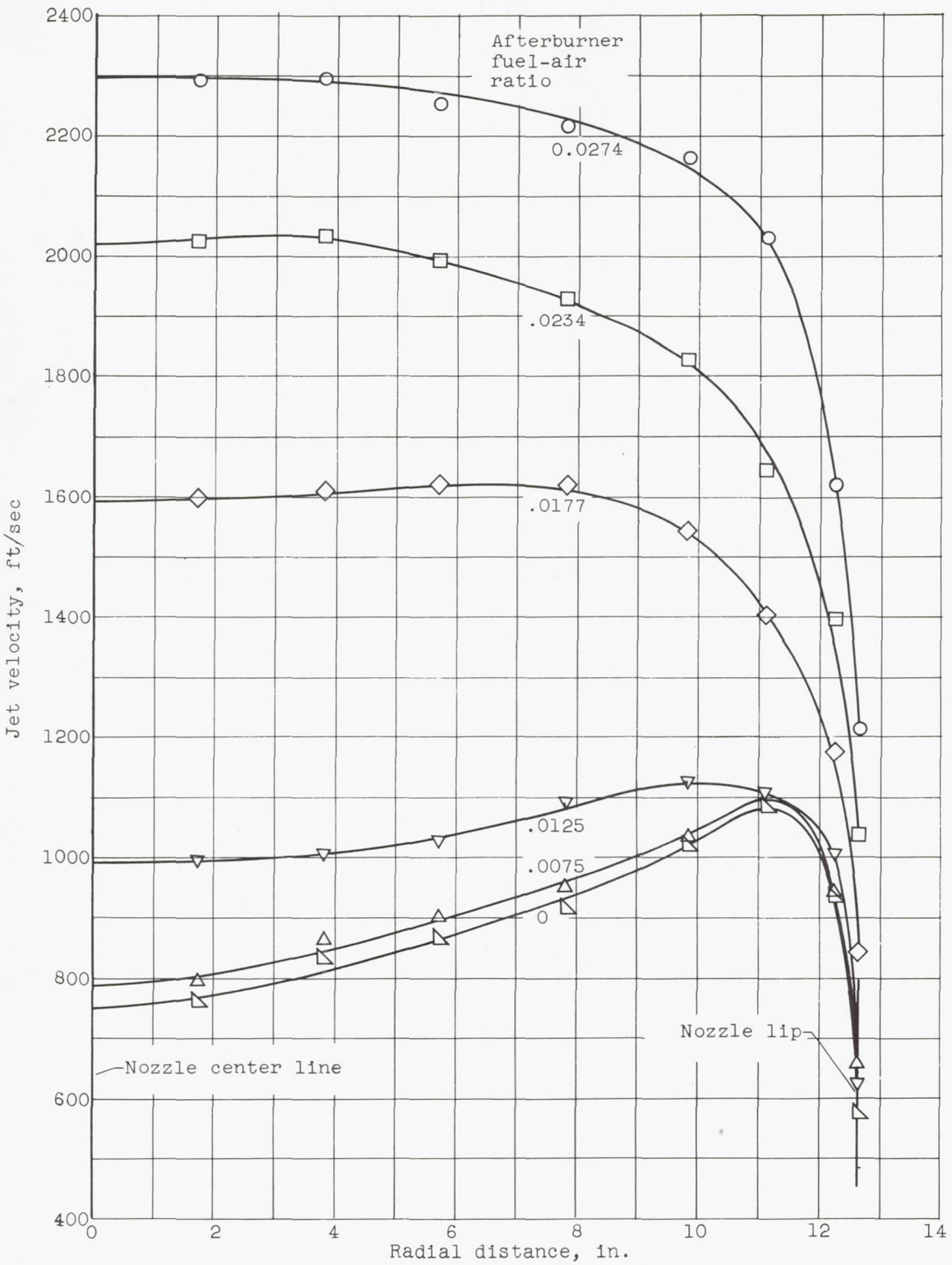

Figure 9. - Velocity profiles at afterburner-nozzle exit.

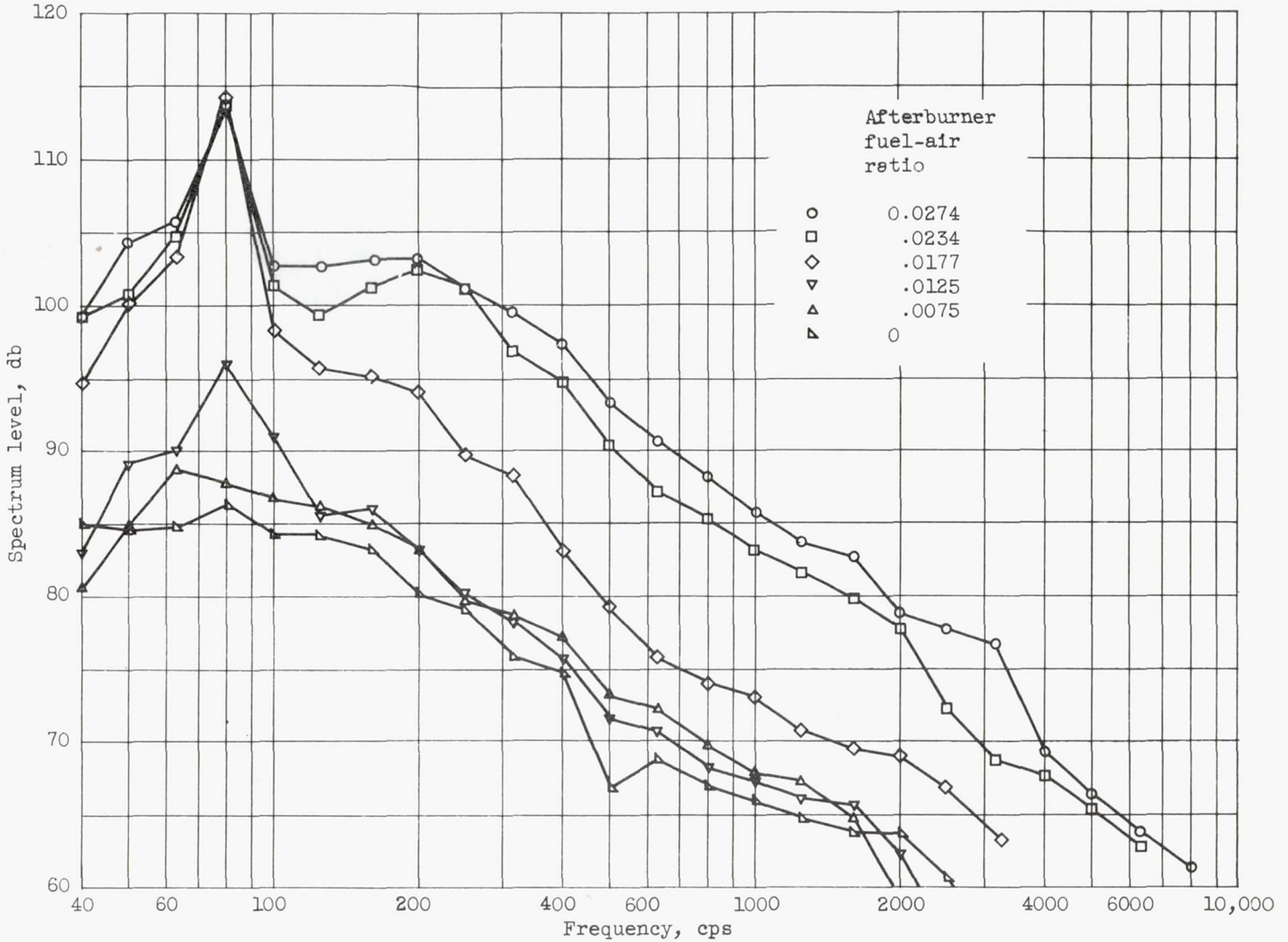

(a) Azimuth angle, 45°.

Figure 10. - Spectrum level for engine-afterburner combination. Distance from jet exit, 200 feet.

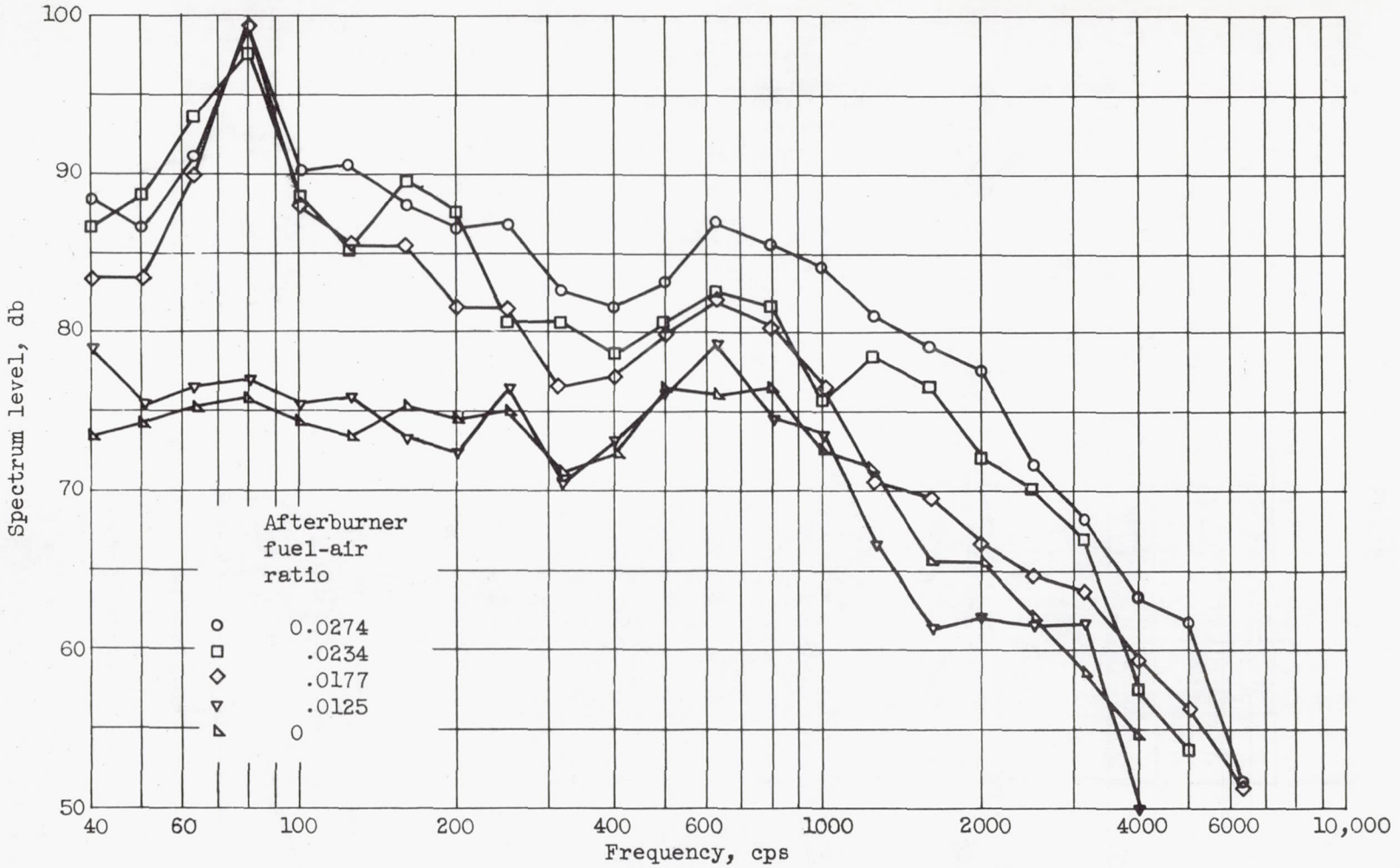

(b) Azimuth angle, 90°.

Figure 10. - Concluded. Spectrum level for engine-afterburner combination. Distance from jet exit, 200 feet.

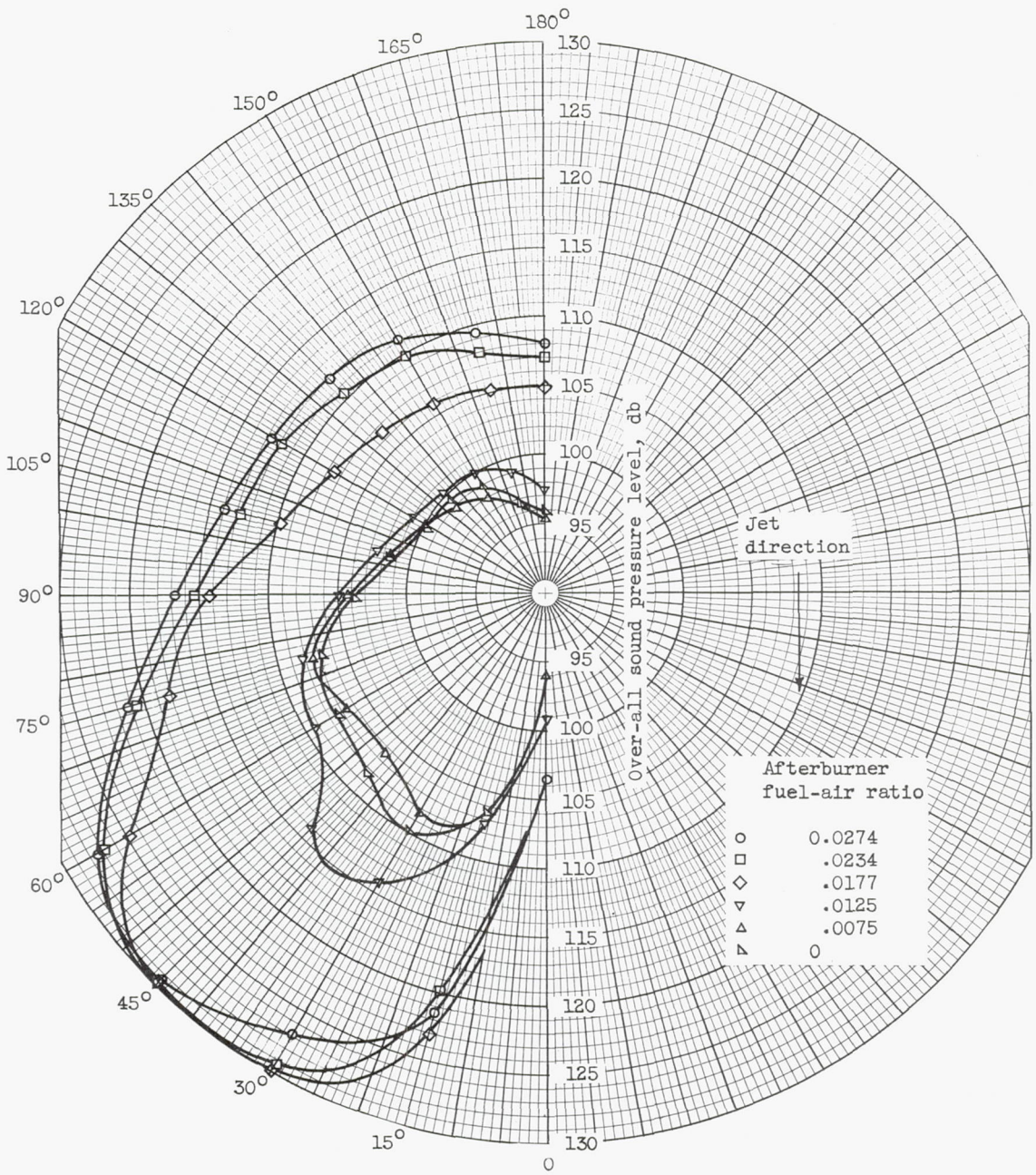

Figure 11. - Polar diagram of sound field for engine-afterburner combination. Distance from jet exit, 200 feet.

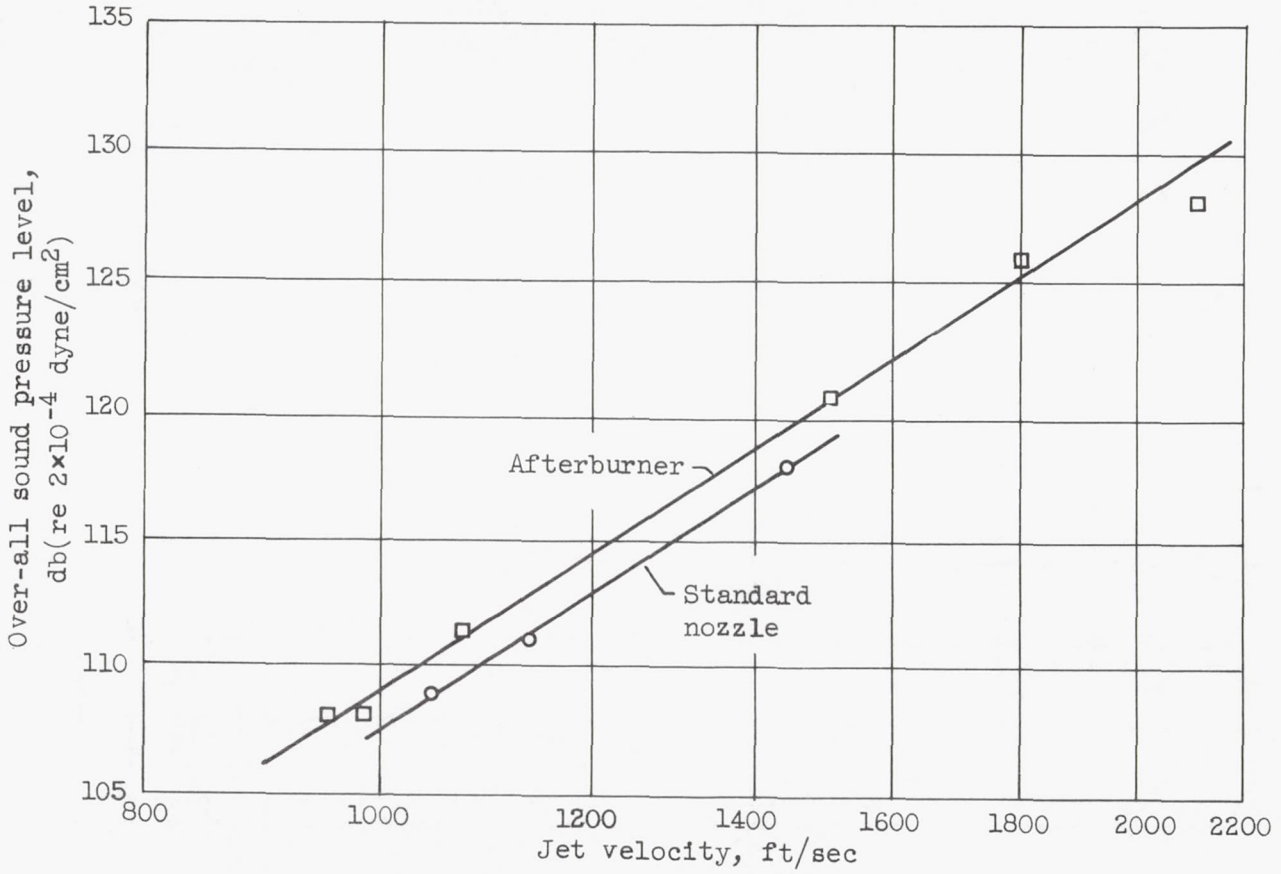

Figure 12. - Variation of over-all sound pressure level with velocity. Azimuth angle, 45°; distance from nozzle, 200 feet.

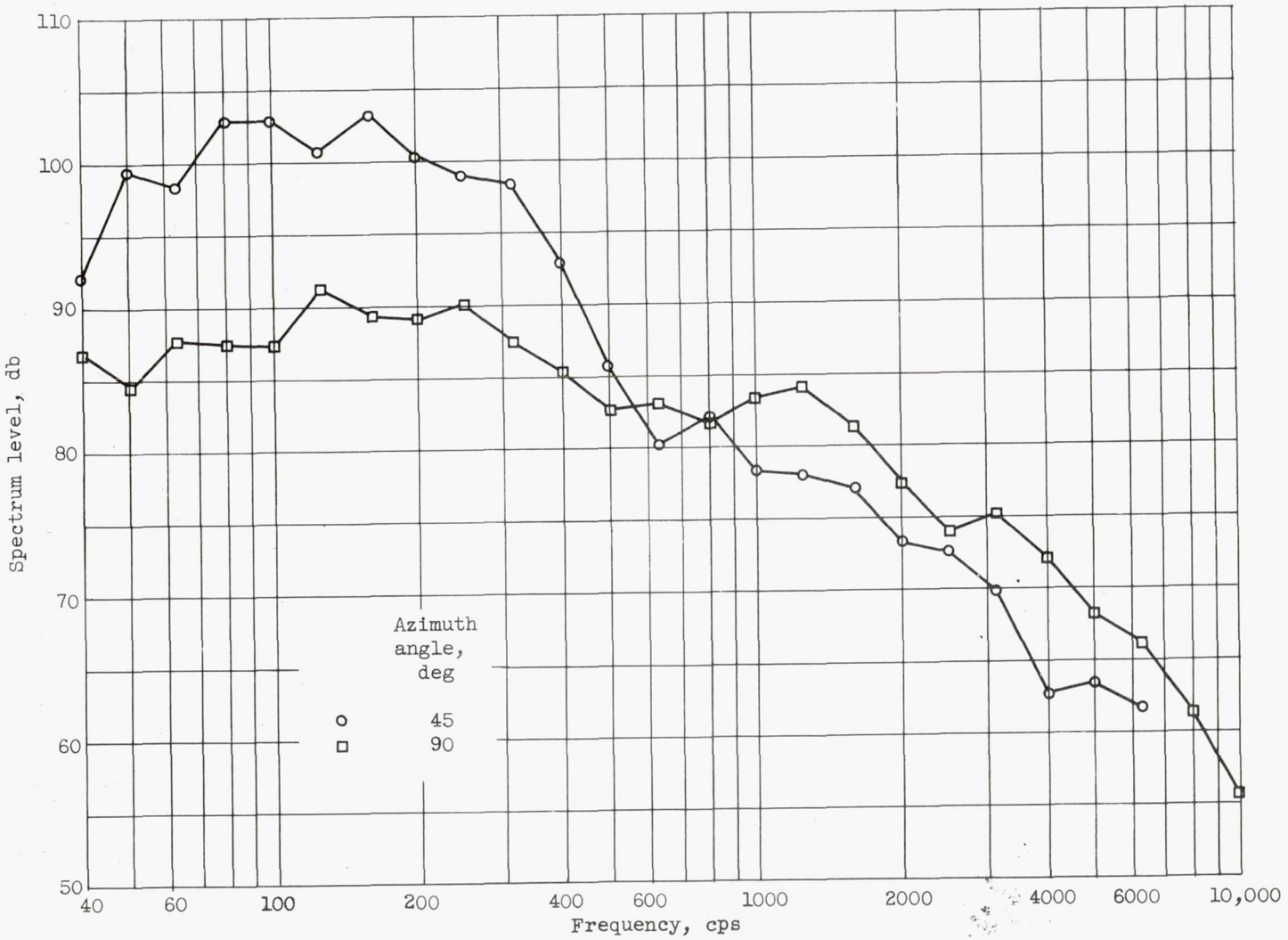

Figure 13. - Spectrum level for fighter aircraft engine installation under maximum afterburner thrust condition. Distance from jet exit, 200 feet.

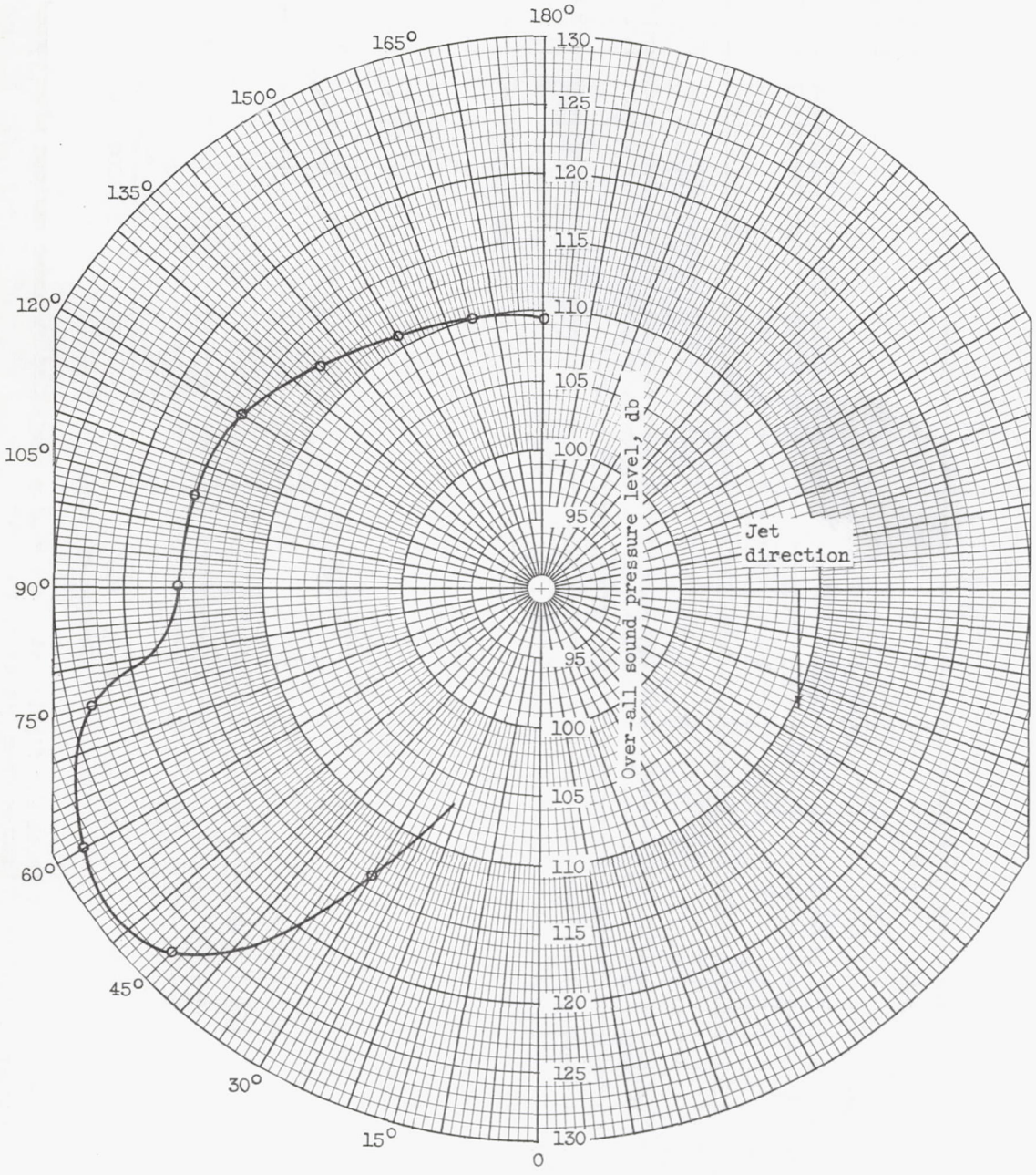

Figure 14. - Polar diagram of sound field for fighter aircraft engine installation under maximum afterburner thrust condition. Distance from jet exit, 200 feet.